A 3-D Volume Coverage Path Planning Algorithm With Application to Intracerebral Hemorrhage Evacuation

Josephine Granna, *Student Member, IEEE*, Isuru S. Godage, *Member, IEEE*, Raul Wirz, *Member, IEEE*, Kyle D. Weaver, Robert J. Webster III, *Senior Member, IEEE*, and Jessica Burgner-Kahrs, *Member, IEEE*

***Abstract*—This letter presents a new heuristic 3-D volume coverage path planning (VCPP) algorithm for robotic intracerebral hemorrhage evacuation. In contrast to existing 3-D planning techniques, the proposed algorithm generates 3-D paths without first decomposing the volume into series of 2-D planning problems. It considers the morphology of the volume to be covered and minimizes the configuration or task space distance traveled. The algorithm merges elements from existing grid-based and wavefront approaches and accommodates kinematic and environmental constraints, as well as obstacle avoidance. We provide both simulation and experimental demonstrations of the algorithm in the context of intracerebral hemorrhage evacuation where a curved, needle-like robot must suction out blood from within the brain by covering the interior of a semicoagulated blood-filled volume with its tip. We perform a simulation study with 7 patient datasets and compare the distance traveled with our new algorithm using a conventional 2-D layer-by-layer planning approach. We also perform 3 *in vitro* evacuation experiments on phantoms made to match patient hemorrhage geometries. Our results illustrate that the VCPP algorithm economizes motion and is more efficient than a layer-by-layer CPP approach.**

***Index Terms*—Medical Robots and Systems, Surgical Robotics, Motion and Path Planning.**

I. Introduction

COVERAGE path planning (CPP) has been a topic of substantial study, since it applies to underwater or land inspections, unmanned aerial vehicles, milling, floor cleaning, painting, and medical tasks, among other robotics applications. Both offline and online CPP algorithms have been previously proposed. The latter can adapt to changing circumstances during execution. Many 2-D CPP algorithms have been proposed. Most are known as *cellular decomposition methods* because they decompose the space to be covered into subregions, which are each then covered separately using simple planning strategies [1]. Online topological cellular decomposition techniques for mobile robots often generate cells based on natural landmarks [2]. Grid-based methods use a collection of uniform grid cells generated using, e.g. wavefront distance transformations [3], spiral paths [4], or neural networks [5]. An early review of CPP methods in robotics was provided by Choset [1], and a more recent review by Galceran & Carreras [6].

A straightforward method of extending 2-D CPP algorithms to 3-D is to decompose the problem into a series of 2-D problems (see e.g. [7]–[9]). Sampling-based approaches compute a path for coverage randomly and compute the minimum cost for the robot to travel along this path before [10] or during [11] execution. Most of the existing *3-D* methods aim to cover a 3-D surface. Existing *volume-based* 3-D CPP algorithms decompose the problem into a series of 2-D layers. Prominent examples are additive manufacturing and milling. For instance, in fused filament fabrication the print head (∼robot) covers the desired volume to be printed in a layer-by-layer approach. The algorithm we propose here does not implement a layer-by-layer approach (we compare its efficiency to that of a layer-by-layer approach later in this letter) and can be applied to any volume coverage problem.

As a practical demonstration of the usefulness of our new approach, we apply it to robot-assisted intracerebral hemorrhage (ICH) evacuation. A patient will have an ICH when a blood vessel in the brain ruptures and blood accumulates in the area surrounding the vessel, forming a cavity of semi-clotted blood called a hematoma. ICHs account for 20% of all strokes, have a 30 day mortality rate of 40%, and a one year mortality rate of 55% [12]. ICHs harm the brain by exerting excessive pressure on surrounding structures, and it is believed that damage to the brain and mortality could be reduced by relieving this pressure. Physicians sometimes attempt surgery to remove the semicoagulated blood (called a hematoma), but this is not generally effective in reducing mortality rates. To provide a less invasive approach to remove the semicoagulated blood, Burgner et al. [13] proposed use of a steerable, needle-like device composed of 2 concentric tubes, the inner of which is curved and elastic (a continuum robot [14]). Coordinated motion of the axial rotation and telescopic insertion of the tubes was used to move the tip of the device within the hematoma. Tip motion is needed because the hematoma consists of semicoagulated blood, and can be removed only locally around the needle tip. The blood is typically not liquid enough at the time removal

Manuscript received August 31, 2015; accepted January 16, 2016. Date of publication February 11, 2016; date of current version March 4, 2016. This paper was recommended for publication by Associate Editor T. Haidegger and Editor K. Masamune upon evaluation of the reviewers comments. This work was supported in part by the National Institutes of Health under award R21 NS087796 and in part by the German Research Foundation under award number BU 2935/1-1.

J. Granna and J. Burgner-Kahrs are with the Hannover Center of Mechatronics, Leibniz Universität Hannover, Hannover 30161, Germany (e-mail: granna@lkr.uni-hannover.de, burgner-kahrs@lkr.uni-hannover.de).

I. S. Godage, Raul Wirz, and R. J. Webster III are with the Department of Mechanical Engineering, Vanderbilt University, Nashville, TN 37212 USA (e-mail: isuru.godage@vanderbilt.edu).

K. D. Weaver is with the Department of Neurological Surgery, Vanderbilt University Medical Center, Nashville, TN 37232-2380 USA.

Digital Object Identifier 10.1109/LRA.2016.2528297

is attempted to be suctioned out from a single needle tip position. Godage et al. then demonstrated a layer-by-layer planning approach that decomposed the 3-D hematoma volume into a series of 2-D planning problems, which were solved using a spiral tip trajectory within each layer [15]. Here, we seek to improve upon the efficiency of the process by aspirating the volume with lower overall robot motion.

The most important contribution of this letter is that this is the first 3-D volume CPP (VCPP) algorithm which considers the complete morphology directly rather than subdividing the problem into a series of 2-D CPP problems. The algorithm minimizes distance traveled by the actuators or tip of the robot. We also contribute an experimental demonstration that in the context of ICH, this new algorithm economizes motion, leading to a more rapid overall procedure for tubular continuum robots.

II. 3-D Volume Coverage Path Planning

A. Problem Statement

Our VCPP algorithm determines a sequence of robot configurations which form the covering path. The covering path visits all positions within a 3-D volume. The input to the algorithm is the environmental information, i.e. the 3-D volume V that the robot should cover in Cartesian space. This volume is represented by its surface points $\boldsymbol{p}$ and can be non-convex. Another input to the algorithm is the robot's starting configuration $\boldsymbol{q}_0$ which corresponds to a pose in Cartesian space within V.

An optional input is the desired final position $\boldsymbol{q}_f$. If $\boldsymbol{q}_f$ is not defined, the robot will stop at an arbitrary configuration. Another optional input is the entry path, i.e. if the robot's kinematic structure enters the volume on a specific path. Depending on the application, a safety margin may be defined, for instance if the robot should avoid areas close to the boundary of the volume. The VCPP algorithm then excludes positions or configurations within this boundary area.

B. Preprocessing Phase

1) Safety Margin: To implement a safety margin δ, the volume to be covered is shrunken towards its centroid $\boldsymbol{c}$. To achieve this, each surface point $\boldsymbol{p}$ is translated toward the centroid by δ:

$$\boldsymbol{p}^* = \boldsymbol{p} + \delta \cdot \frac{\boldsymbol{c} - \boldsymbol{p}}{|\boldsymbol{c} - \boldsymbol{p}|} \,. \tag{1}$$

Alternatively, scaling the object by a defined percentage could be realized using homogeneous transformation or surface normals.

We note that highly non-convex volumes or large safety margins require special consideration in order to preserve the topology, e.g. discrete scale axes representations [16].

2) Grid Establishment: Prior to computation of the covering path, the surface representation is converted into a volumetric representation with isotropic voxel size. Each voxel within V is set to *one* and each outside voxel is set to *zero*. If obstacles are present within the environment, they are either assigned *zero* or another value if differentiation from the area outside V is required (e.g. if parts of the robot structure are allowed to be outside of the coverage volume, but still must avoid obstacles). The VCPP problem can now be considered a sequence of robot configurations that visit each voxel assigned to *one* at least once.

3) Determine Reachable Space: In this third preprocessing step, each voxel is evaluated to determine whether it is, in principle, reachable by the robot using inverse kinematics. If a voxel is not reachable (i.e. the robot's workspace does not fully cover the desired coverage volume), it is tagged as *unreachable* by the algorithm. A voxel is also tagged as *unreachable*, if reaching it would require collision with an obstacle or intersection of any part of the robot with a position outside the desired coverage volume. The collision detection algorithm should be chosen based on the specific application and kinematic structure of the robot (the interested reader is referred to [17]). In summary, after this last preprocessing step, all reachable voxels are assigned a corresponding robot configuration $\boldsymbol{q}_i$. The number of reachable voxels is denoted with m.

The ratio of the number of voxels reachable by the robot to the number of voxels not reachable (either due to kinematic constraints or collisions) expresses the percentage of f_{cov} of V which can be covered. We note, that this preprocessing step makes the implicit assumption that all reachable voxels are reachable from all others, i.e. no collisions of the robot with obstacles occur and the boundary of the volume is not passed during motion. Collision checking as well as consideration of redundant robot configurations leading to a reachable voxel are explicitly considered in the path planning algorithm. Thus, the actual f_{cov} may be lower than estimated in this preprocessing step.

C. 3-D Volume Coverage Path Planning Algorithm

We now seek for the sequence G of robot configurations $\boldsymbol{q}_i$ to cover the 3-D volume. The robot starts at configuration $\boldsymbol{q}_0$ with end effector position $\boldsymbol{p}_0 = [x_0\, y_0\, z_0]$. Inspired by the wavefront CPP algorithms, we introduce spherical wavefronts originating from the initial position $\boldsymbol{p}_0$ of the robot. Fig. 1(top) illustrates the approach. To favor robot configurations with end effector positions close to the current end effector position, we use N spherical intervals $I = \{[0, d], \ldots, [(N-1) \cdot d, N \cdot d]\}$, where the radius of the spherical intervals increases by d for each interval. The number N of spherical intervals is chosen such that the sphere with radius $N \cdot d$ contains V completely (see Fig. 1(top, right)). The spherical intervals are considered sequentially by the planner.

To quantify the cost of traveling from one configuration to another, we define the following cost function in configuration space:

$$c(\boldsymbol{q}_i, \boldsymbol{q}_j) = \boldsymbol{\lambda} \cdot |\boldsymbol{q}_j - \boldsymbol{q}_i| \,, \tag{2}$$

with $\boldsymbol{q}_i$ the current robot configuration, $\boldsymbol{q}_j$ the desired robot configuration, $\boldsymbol{\lambda} \in \mathbb{R}^n$ assigning weights to each configuration space parameter of the robot such that $|\lambda| = 1$, and n dimension of the robot's configuration space. We note that our algorithm currently does not specify anything about the tip path of the robot between voxels. It is in principle possible to

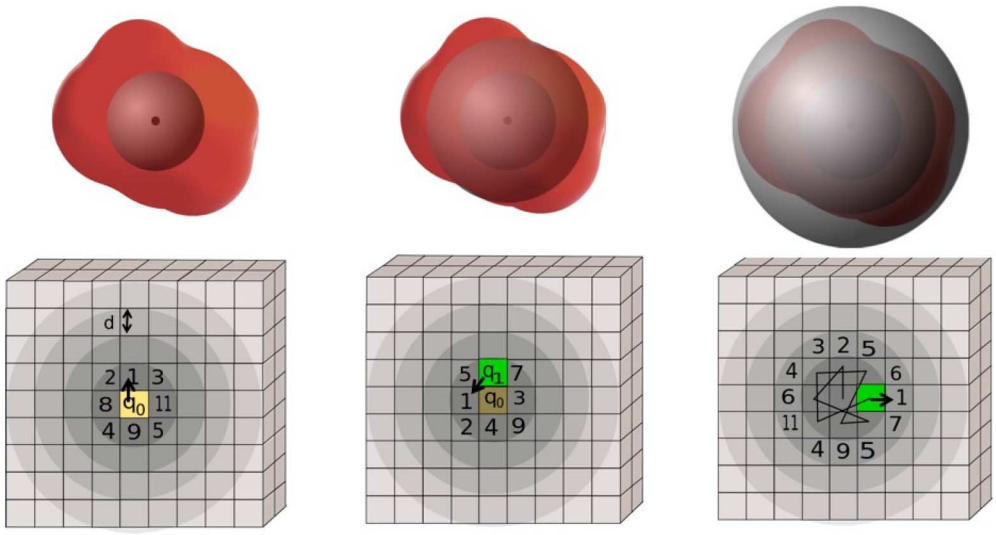

Fig. 1. 3-D volume coverage path planning algorithm with spherical intervals around starting configuration q_0 and cost function assigned to all voxels within the spherical wave ranges (illustrated by greyscales) in relation to the current robot configuration in order to ensure minimum actuator traveling distances.

use a cost function that includes Cartesian travel distance, or smoothness of the trajectory, if the application requires explicit consideration of such factors.

The planner determines G stepwise and considers all *reachable* voxels within the current interval I_i at once. The cost function c is evaluated and assigned to all unvisited reachable voxels within the current interval in relation to $\boldsymbol{q}_i$. Then, the robot configuration $\boldsymbol{q}_j^*$ leading to the minimum cost $c(\boldsymbol{q}_i, \boldsymbol{q}_j^*)$ is added to G, the corresponding voxel is marked as *visited*, and $\boldsymbol{q}_i = \boldsymbol{q}_j^*$ for the next step. If multiple voxels are assigned with the same minimum cost, $\boldsymbol{q}_j^*$ is chosen randomly from all configurations corresponding to the minimum cost. In presence of obstacles or required avoidance of the volume boundary, the algorithm must check if the motion of the robot from $\boldsymbol{q}_i$ to $\boldsymbol{q}_j^*$ is collision free. If not, the voxel corresponding to $\boldsymbol{q}_j^*$ is reset to *unreachable* and a configuration with second least cost is checked (and so on). If none of the remaining reachable voxels results in collision free motion, they are marked as *unreachable*. Note that if a robot structure provides redundant configurations for a given voxel, the one with the least change in actuator values should be selected by the algorithm.

If all voxels within the current interval are marked as visited, i.e. corresponding robot configurations have been added to G, the planner proceeds to the next interval. This process is illustrated in Fig. 1(bottom). After the planner finished with the last interval, the 3-D volume coverage path is given as as the sequence

$$G = \{\boldsymbol{q}_0, \boldsymbol{q}_1, \ldots, \boldsymbol{q}_m\} \tag{3}$$

of robot configuration parameters. If a final configuration is desired, then $q_m = q_f$.

III. Application to ICH Evacuation

This section describes the application of the proposed 3-D volume coverage path planning algorithm to robot-assisted intracerebral hemorrhage evacuation. In intracerebral hemorrhage evacuation, a tubular aspiration robot composed of 2 concentric tubes is used to enter the volume of the hematoma caused by the hemorrhage with a specific entry path and evacuate blood via coordinated telescopic motion of both tubes and axial rotation of the inner tube.

We aim for the robot's tip to visit the whole volume of the hemorrhage, as the accumulated blood is coagulated. Depending on the time passed since the ICH occurence and diagnosis to the beginning of the treatment, the coagulated blood's consistency is in between liquid and gel. Thus, it can be assumed that only a small volume of blood is aspirated at the robot's tip. Since surrounding brain tissue should not be damaged, the robot should avoid areas in proximity to the edges of the hematoma and should never leave the volume. To reduce the surgical procedure time, we desire rapid evacuation, yet maximum total coverage. While rapid evacuation is dependent on several parameters (aspiration, degree of coagulation, etc.), in this letter we solely consider low incremental changes in actuator displacement. We note that a future version of the motion planner will include other parameters such as brain deformation and the state of the coagulation.

1) Robot System

The robot system is illustrated in its experimental setup in Fig. 2. It consists of the actuation unit, concentric tubes, a passive lockable articulated arm used to position the robot over the patient's head, a trajectory guide to adjust the entry vector of the needle, and an aspirator, which is attached to the inner tube for blood evacuation. The robot is placed within a CT scanner for pre- and postoperative imaging. Prior to evacuation, the surgeon selects the inner aspirating tube from a tube set with different tube radii r available in the operating room. One way to choose the tube with the best radius of curvature r from among a set of options is to use our previously presented optimization algorithm [18], [19]. If coverage of the hemorrhage with a single tube is lower than the surgeon desires, a second tube can be

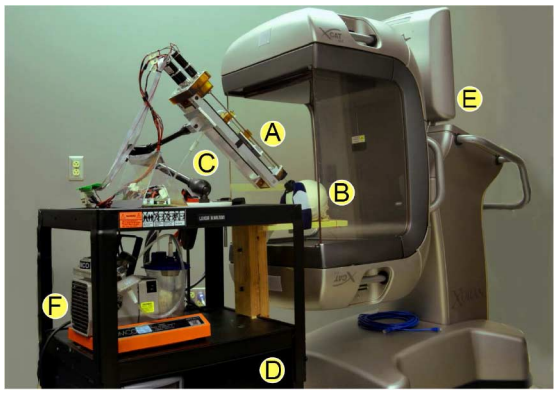

Fig. 2. The experimental setup: (A) the robot inserted through a burr hole on top of the skull, (B) the brain phantom, (C) the lockable positioning arm holding the robot, (D) Simulink Realtime system, (E) the Xoran xCAT CT scanner, and (F) the vacuum pump.

introduced after the first has removed all the material it can reach.

A. Configuration Space

The inner tube of the tubular aspiration robot is composed of a straight section with length L_{s1} and a curved section L_c. The outer straight tube with length L_{s2} is used to reach the hematoma on a direct path. Configuration parameters are the translation of the inner and outer tube, denoted with β_1 and β_2 and the rotation of the inner tube α. The translational parameters are negative as they represent the distance of the tube's proximal end from the restrained outlet of the tubes which marks the origin. The configuration parameters are illustrated in Fig. 3(left). The 3-D coverage motion planner thus needs to determine a sequence of configuration parameters $q = [\beta_1\, \beta_2\, \alpha]$ of the robot.

B. Inverse Kinematics

In this letter, we use a geometric inverse kinematic model which determines $\boldsymbol{q} = \text{invKin}(x, y, z)$. The inverse model is based on the geometric forward kinematic model described in [18]. First, the lengths ℓ_1, ℓ_2 are computed based on the desired end effector position of the robot $[x\, y\, z]$, as illustrated in Fig. 3(right). ℓ_1 is the extended outer tube length measured from the front plate of the robot to the tip of the outer tube. ℓ_2 denotes the curved length of the inner tube. The rotation α of the aspiration tube can be computed by determining the relative angle between the x- and y-axis of the robot coordinate system. The translational parameters can be determined as

$$\beta_1 = \ell_2 + \beta_2 + L_{s2} - L_{s1} - L_c\,, \tag{4}$$

$$\beta_2 = -L_{s2} - \ell_1\,, \tag{5}$$

with

$$\ell_1 = z - \frac{\sin(\kappa \cdot \ell_2)}{\kappa}\,, \tag{6}$$

$$\ell_2 = \frac{1}{\kappa} \arccos\left(\frac{-x \cdot \kappa}{\sin\alpha} + 1\right)\,, \tag{7}$$

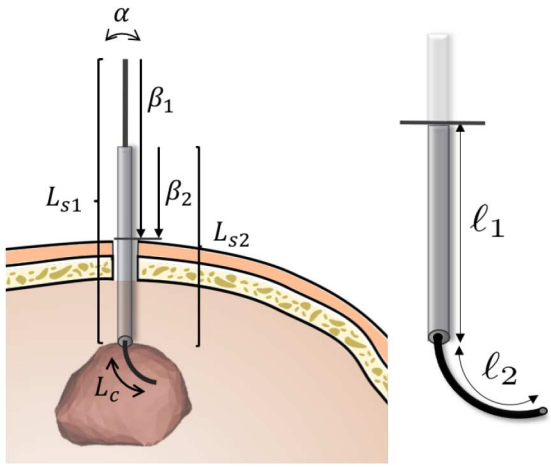

Fig. 3. Configuration parameters β_1, β_2, α and lengths L_{s1}, L_c, L_{s2} of tubular aspiration robot.

where $\kappa = r^{-1}$ denotes the curvature of the inner tube. If α is equal to $0, \pi$ or 2π ℓ_2 is determined with

$$\ell_2 = \frac{1}{\kappa} \arccos\left(\frac{y \cdot \kappa}{\cos\alpha} + 1\right)\,. \tag{8}$$

The constraints on the configuration space parameters are

$$\beta_1 \in [\beta_2 - (L_c + L_{s1} - L_{s2})]\,, \quad \beta_2 \in [-L_{s2}, 0]\,. \tag{9}$$

C. 3-D Volume Coverage Path Planning for ICH Evacuation

The 3-D volume coverage path planning algorithm described in Section II is applied to robot-assisted ICH evacuation. The input volume can be determined from medical imaging by segmenting the hematoma. The entry path direction into the patient's head (which is defined by the surgeon based on the patient's anatomy) and the entry point onto the skull are used as inputs to the VCPP algorithm.

For the remainder of this letter, the starting configuration $\boldsymbol{q}_0$ is chosen such that the tip position is at (or close to) the centroid c of the hematoma. We note that $\boldsymbol{q}_0$ can be arbitrarily chosen as long as the corresponding robot tip position is within the hematoma. A safety margin δ is used to prevent the robot from moving too close to the brain tissue surrounding the hematoma, in order to prevent additional trauma or the accidental suctioning of brain tissue. δ is defined by the surgeon. The inverse kinematics model described in Section III-B is applied to determine robot configurations that reach voxels within the hematoma. A check on each configuration is performed in order to exclude all configurations where the extended length of the aspiration tube ℓ_2 goes beyond the boundary of the hematoma.

To reduce the overall execution time, we aim to minimize the overall change in actuator displacement, as procedure time and traveled actuator distance are highly correlated for tubular robots. The cost function of the 3-D volume CPP algorithm (Eq. (2)) becomes

$$c(\boldsymbol{q}_i, \boldsymbol{q}_j) = \lambda_1 \cdot (\beta_{1j} - \beta_{1i}) + \lambda_2 \cdot (\beta_{2j} - \beta_{2i}) + \lambda_3 \cdot (\alpha_j - \alpha_i)\,. \tag{10}$$

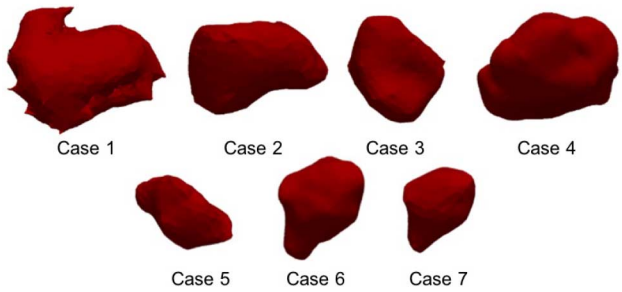

Fig. 4. Surface data of hemorrhages segmented from computed tomography datasets of 7 real patients.

To normalize translational and rotational units, the rotational difference α is converted into a tip distance traveled in millimeters before use in the equation above.

IV. Simulation Experiments

A. Simulation Data

To evaluate the performance of the proposed 3-D volume coverage path planning algorithm in the context of intracerebral hemorrhage evacuation, we applied it to a total of 70 patient cases (i.e. unique hematoma geometries and/or unique entry trajectories) in simulation. To perform these simulation experiments, we segmented the volume of 7 real patient intracerebral hemorrhage cases from computed tomography datasets using 3-D Slicer (http://www.slicer.org/) and exported the hematoma as surface data. Fig. 4 shows the hematoma geometries. The volumes of these hematomas are 72, 39.7, 35.5, 34.7, 16.9, 16.3, 13.3 ml respectively. For each patient case, we generated 10 random entry paths, resulting in 70 simulated patient cases. The safety margin was set to $\delta = 5\,\text{mm}$.

B. Parameters

For the simulation experiments we choose the straight inner tube length $L_{s1} = 160\,\text{mm}$, curved inner tube length $L_c = r_i \cdot \pi\,\text{mm}$, and straight outer tube length $L_{s2} = 160\,\text{mm}$ to match the physical robot used for *in vitro* experiments described in the following section. We use an aspiration tube set of 4 radii of curvature: $r = \{17, 19, 21, 23\}\text{mm}$. We then apply the VCPP algorithm as described in Section III-C to each of the 70 cases and each r. Thus, a total of 280 simulation experiments are performed. We note that one could utilize the optimization algorithms we proposed in [18] and [19] to obtain the radius of curvature of the aspiration tube which results in maximum coverage. In this letter, we are concerned with coverage path planning for a given tube rather than finding the tube with the best coverage.

Voxel size was set to 1mm (chosen based on the inner diameter of the curved tube), $N = 10$ intervals I are chosen empirically with radius increase d, computed by determining the rounded up maximum Euclidean distance to all surface points from the center of mass c and dividing it by N. The weighting factors of the cost function (Eq. (10)) are assigned $\lambda_1 = 0.7$, $\lambda_2 = 0.15$, and $\lambda_3 = 0.15$ in order to reduce the rotational difference between configurations. If the Euclidean distance between the tip positions of two configurations is $> 15\,\text{mm}$, intermediate configurations of the inner and outer tube are added to the motion plan. These intermediate configurations resemble retraction of the tubes toward the point at which the tubes entered the hematoma, with no rotational change, in order to prevent the robot from penetrating through the hematoma's boundary during motion.

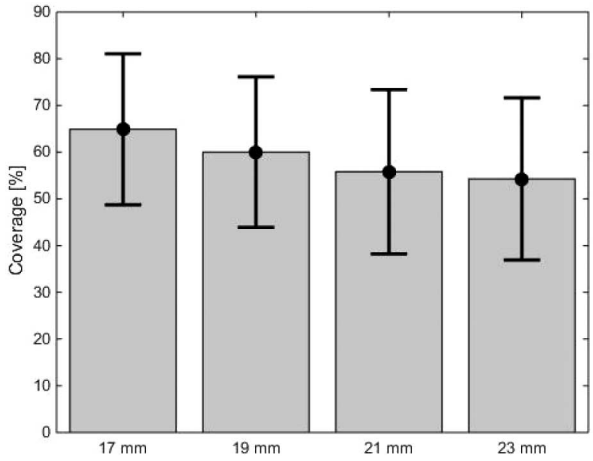

Fig. 5. Mean coverage and standard deviation over 70 cases for aspiration tube radii of curvature $r = \{17, 19, 21, 23\}$ mm.

C. Evaluation

For each case, we evaluate coverage f_{cov}, computation time t, overall distance traveled in configuration space

$$dist_Q(G) = \sum_{i=1}^{m-1} |\boldsymbol{q}_{i+1} - \boldsymbol{q}_i| \,. \tag{11}$$

We further determine the overall distance traveled by the aspiration tube's tip in Cartesian space $dist_{\mathbb{R}^3}(G)$. Therefore, we compute the course of tip positions using the forward kinematics model as described in [18] for synchronous Point-to-Point motion between the configurations in G [20].

These results will be compared to a conventional layer-by-layer algorithm, which covers the hematoma starting from the entry point, and proceeding to the opposite side of the hematoma. The spiraling path is computed clockwise from the initial voxel, which lies along the needle's entry vector, toward the boundary for each layer.

D. Results

The mean coverage and standard deviation over 70 cases for an aspiration tube with each radius of curvature in $r \in \{17, 19, 21, 23\}\text{mm}$ is illustrated in Fig. 5.

We ran the layer-by-layer CPP and VCPP algorithm on each patient case for each aspiration tube on an Intel Core i7-4790 3.60 GHz implemented in Matlab making use of parallel processing. The computation time for both algorithms is comparable: the mean computation time over all 280 experiments

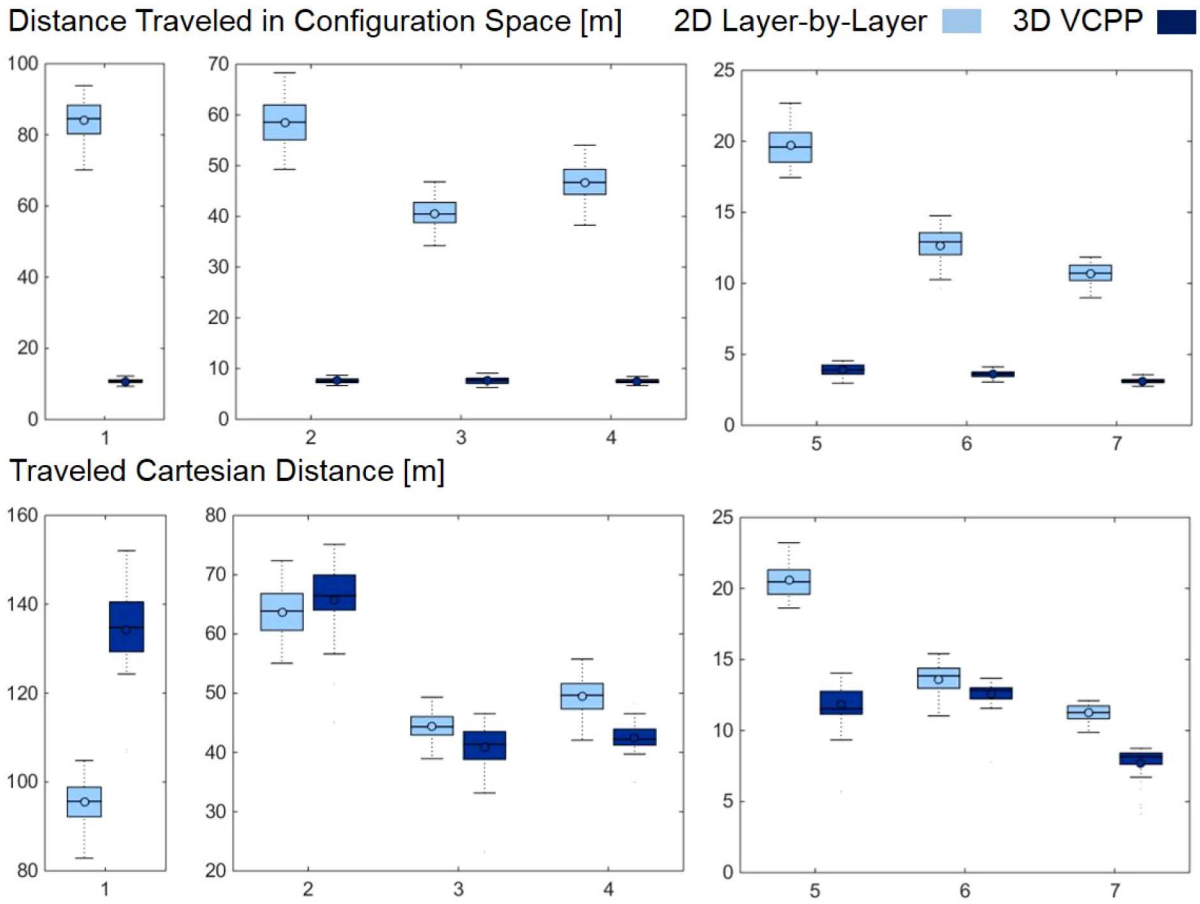

Fig. 6. Boxplots of simulation results grouped by case. The central mark is the median, the edges of the box are the 25th and 75th percentile, and the whiskers extend to the most extreme data points not considered outliers (outliers are defined beyond $\pm 2.7\sigma$). Layer-by-layer CPP results are indicated in light blue, VCPP in dark blue. Please note that the y-axis varies in scaling for case 1, cases 2-4, and cases 5-7. Traveled distances in configuration space (top) and corresponding traveled distances by tube tip in Cartesian space (bottom).

for the CPP is $4.48\,\text{s} \pm 4.03\,\text{s}$, with minimum time 0.69 s, and maximum time 14.42 s. For the VCPP mean computation time is $4.90\,\text{s} \pm 4.32\,\text{s}$, minimum time 0.88s, and maximum time 15.02 s. The computation time is case specific and dependent on the size of the hemorrhage volume. A dedicated implementation in C++ will likely result in computation times less than 1 s.

The overall distances traveled in configuration space $dist_Q(G)$ and Cartesian space $dist_{\mathbb{R}^3}(G)$ for the layer-by-layer CPP and our VCPP are summarized in Fig. 6. On each box, the central mark is the median, the edges of the box are the 25th and 75th percentile, and the whiskers extend to the most extreme data points not considered outliers (outliers are defined beyond $\pm 2.7\sigma$). We can observe in the top row of Fig. 6 that the VCPP always outperforms the layer-by-layer algorithm in terms of overall traveled distances in configuration space. As the cost function we applied did not optimize for the traveled distance of the robot tip in Cartesian space, we can observe for the largest hematoma (case 1 with volume 72 ml) that the VCPP results in considerably larger distances. This is not the general case as we can see for cases 2-7. In fact, the VCPP performs similar or better than the layer-by-layer CPP.

V. In Vitro Experiments

To experimentally evaluate our proposed 3-D volume coverage path planning algorithm for ICH evacuation, we performed experiments with phantom gelatin models based on real patient medical images. Two phantom models were generated by using rapid prototyping to obtain a printed mold of the patient hematoma and casting gelatin into the printed mold. Barium Sulfate ($BaSO_4$) contrast agent was added to create the hematoma gelatin model. After curing the gelatin, the hematoma was taken out of the mold and placed into a synthetic plastic skull which was then filled with plain gelatin. Fig. 7 shows a phantom skull equipped with a molded hematoma of red gelatin for illustration.

Fig. 7. Phantom gelatin model of an intracerebral hemorrhage (red) within a plastic skull and a steerable cannula for blood evacuation.

TABLE I
EXPERIMENTAL RESULTS. PREOPERATIVE AND POSTOPERATIVE VOLUME [ML], ACHIEVED COVERAGE [%] AND DURATION TIME [MIN]

Experiment	Pre-Op Vol.	Post-Op Vol.	Coverage	Time
1	30.14	11.29	63%	40
2	34.06	5.13	85%	30.5
3	34.16	3.75	89%	20.3

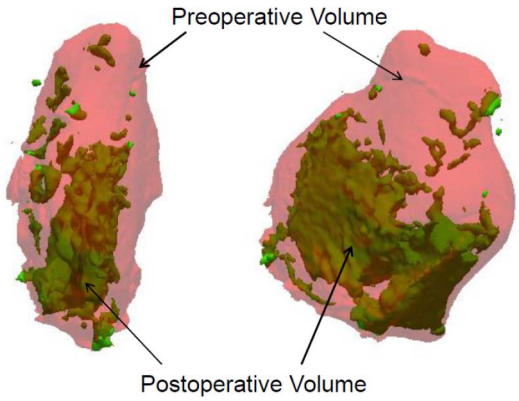

Fig. 8. Two views on 3-D rendering of pre- (red) and postoperative (green) hematoma volume of in vitro experiment 3.

The robot system was set up with the phantom skull containing the gelatin model and held securely in place on a wooden platform with elastic bands. A CT image dataset was acquired and the robot was aligned such that the tubes pointed approximately at the center of the hematoma. The hematoma volume was then segmented using 3-D Slicer and this segmentation was used as an input to the path planning algorithm. The entry vector and entry point on the skull were also determined in the CT images. The 3-D path plan was then computed using the parameters of physical tubes attached to our robot, which were: $r = 17.62\,\text{mm}$, $L_{s1} = 160\,\text{mm}$, $L_c = 49.5\,\text{mm}$, and $L_{s2} = 160\,\text{mm}$.

Three experiments were performed, using two different anatomical patient hematoma models. On one model, two different entry paths were considered. Planning was then conducted as described in Section III-C. Robot motion was controlled using the Matlab Simulink Real-Time interface.

The entry vector was next measured from a CT scan of the robot skull phantom. In all the experiments, a 5 mm safety margin was applied around the periphery of the hematoma to account for tissue deformation. The curved tube was confined to the interior of the hematoma. The tip of the robot was actuated at a velocity of 2.5 mm/sec. The pre- and postoperative volume, the coverage and experimental duration time are shown in Table I. Fig. 8 and Fig. 9 illustrate results of experiment 3.

VI. DISCUSSION

Our VCPP algorithms enables computation of volume covering paths in general non-convex volumes by minimizing a cost function. As seen in the results in Section IV, the cost function can optimize overall traveled distance in actuator space. This would lead to energy efficient paths covering the volume. On the other hand, if one seeks to minimize the overall traveled distance in Cartesian space, the cost function could be adjusted (as in Eq. 2). In direct comparison, our new algorithm outperforms the layer-by-layer CPP. Our proposed greedy approach could be extended in the future to search for a global optimal path. While we have used the VCPP algorithms for offline path planning, we note that the computation times achieved in Section IV are also fast enough for online application.

The proposed 3-D VCPP algorithm could be extended to other robots, if the inverse kinematics model and spatial extent of the robot are known. The cost function (Eq. 2) needs to be adjusted according to the configuration parameters of the specific robot structure and weights have to be chosen based on the application.

In interpreting the experimental in vitro results, it should be noted that experiment 1 used gelatin that was much softer than that used in experiments 2 and 3, because the sample had been allowed to warm to room temperature for a period of time before the experiment commenced. Experiments 2 and 3 were conducted with cool gelatin that had just been removed from the refrigerator. This affected tissue deformation during the experiment, and no local voids formed within the hematoma in experiment 1, whereas local voids did form in experiments 2 and 3. It remains to be seen how in vivo brain will behave under similar circumstances.

It is also noteworthy that in the in vitro results we achieved, coverage is higher than that estimated by the VCPP. This is due to the fact that the aspiration tube actually removes more than the volume of a single voxel around its tip. Thus, the VCPP is underestimating the actual coverage. We note that the thickness of the safety margin, exact speed of the robot's tip, and other parameters (e.g. aspiration pressure) are somewhat arbitrary, and were simply set to numbers that worked well in our gelatin phantoms, and future work will be needed to determine optimal values to be used in human cases considering brain mechanical parameters and deformation models.

VII. CONCLUSION

We have presented a new volume coverage planning algorithm that acts on the morphology of the volume to be covered directly, rather than subdividing it into a series of 2-D layers and planning paths within them. This algorithm applies to general non-convex volumes and other robot kinematic structures, provided their forward and inverse kinematics are solvable. We applied the new VCPP algorithm to the important practical medical problem of brain decompression for intracerebral hemorrhage patients. Our results illustrate that the new VCPP algorithm is more efficient than traditional layer-by-layer approaches. To further improve the 3-D VCPP algorithm, trajectory generation between configurations should be considered in the future.

With respect to the application of the 3-D VCPP algorithm described in this letter to ICH, future work is necessary to fully account for tissue deformation during aspiration. The approach we envision is described in [15], where iterative intraoperative imaging and re-planning is used to account for tissue deformation. Each time a new image is collected, the motion

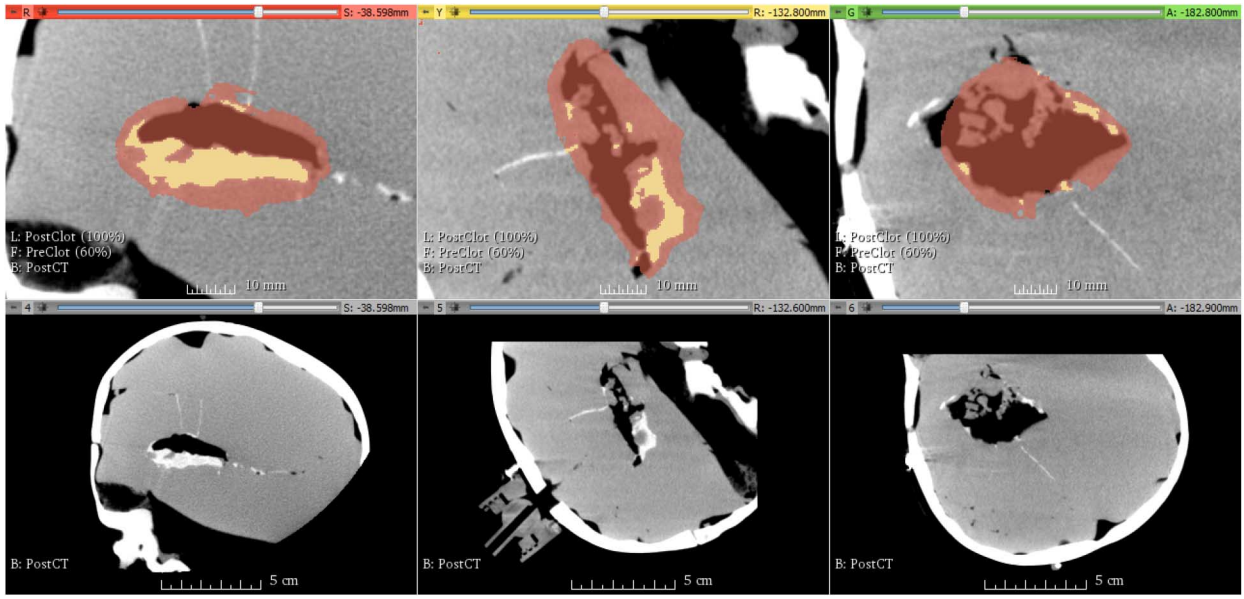

Fig. 9. Screenshot from 3-D Slicer showing the CT image planes of experiment 3 (bottom row) and views zoomed in to the hematoma with pre- and postoperative segmentation overlays (top row). The light brown color shows the original hemorrhage volume, the yellow color denotes the remaining hemorrhage volume after suction and the dark brown color shows the successfully removed volume (top row).

planning results in this letter can be re-applied to generate a new aspiration plan, based on the current deformation state of the brain.

REFERENCES

[1] H. Choset, "Coverage for robotics—A survey of recent results," *Ann. Math. Artif. Intell.*, vol. 31, no. 1, pp. 113–126, 2001.

[2] S. C. Wong and B. A. MacDonald, "A topological coverage algorithm for mobile robots," in *Proc. IEEE Int. Conf. Robot. Autom.*, 2001, pp. 1685–1690.

[3] A. Zelinsky, R. A. Jarvis, J. C. Byrne, and S. Yuta, "Planning paths of complete coverage of an unstructured environment by a mobile robot," in *Proc. Int. Conf. Adv. Robot.*, 1993, pp. 533–538.

[4] Y. Gabriely and E. Rimon, "Competitive on-line coverage of grid environments by a mobile robot," *Comput. Geom.*, vol. 24, pp. 197–223, 2003.

[5] Y. Guo and M. Balakrishnan, "Complete coverage control for nonholonomic mobile robots in dynamic environments," in *Proc. IEEE Int. Conf. Robot. Autom.*, 2006, pp. 1704–1709.

[6] E. Galceran and M. Carreras, "A survey on coverage path planning for robotics," *Robot. Auton. Syst.*, vol. 61, no. 12, pp. 1258–1276, 2013.

[7] S. Hert, S. Tiwari, and V. Lumelsky, "A terrain-covering algorithm for an AUV," *Auton. Robots*, vol. 3, pp. 91–119, 1996.

[8] P. N. Atkar, H. Choset, A. A. Rizzi, and E. U. Acar, "Exact cellular decomposition of closed orientable surfaces embedded in R3," in *Proc. IEEE Int. Conf. Robot. Autom.*, 2001, pp. 699–704.

[9] P. Cheng, J. Keller, and V. Kumar, "Time-optimal UAV trajectory planning for 3-D urban structure coverage," in *Proc. IEEE/RSJ Int. Conf. Intell. Robots Syst.*, 2008, pp. 2750–2757.

[10] B. Englot and F. S. Hover, "Sampling-based sweep planning to exploit local planarity in the inspection of complex 3-D structures," in *Proc. IEEE Int. Conf. Intell. Robots Syst.*, 2012, pp. 4456–4463.

[11] G. Papadopoulos, H. Kurniawati, and N. M. Patrikalakis, "Asymptotically optimal inspection planning using systems with differential constraints," in *Proc. IEEE Int. Conf. Robot. Autom.*, 2013, pp. 4111–4118.

[12] C. J. van Asch, M. J. Luitse, G. J. Rinkel, I. van der Tweel, A. Algra, and C. J. Klijn, "Incidence, case fatality, and functional outcome of intracerebral haemorrhage over time, according to age, sex, and ethnic origin: A systematic review and meta-analysis," *Lancet Neurol.*, vol. 9, no. 2, pp. 167–176, 2010.

[13] J. Burgner, H. B. Gilbert, and R. J. Webster, III, "On the computational design of concentric tube robots: Incorporating volume-based objectives," in *Proc. IEEE Int. Conf. Robot. Autom.*, 2013, pp. 1185–1190.

[14] J. Burgner-Kahrs, D. C. Rucker, and H. Choset, "Continuum robots for medical applications: A survey," *IEEE Trans. Robot.*, vol. 31, no. 6, pp. 1261–1280, Dec. 2015.

[15] I. S. Godage, A. A. Remirez, R. Wirz, K. D. Weaver, J. Burgner-Kahrs, and R. J. Webster, III, "Robotic intracerebral hemorrhage evacuation: An in-scanner approach with concentric tube robots," in *Proc. IEEE/RSJ Int. Conf. Intell. Robots Syst.*, 2015, pp. 1447–1452.

[16] B. Miklos, J. Giesen, and M. Pauly, "Discrete scale axis representations for 3-D geometry," *ACM Trans. Graph.*, vol. 29, no. 4, pp. 101:1–101:10, 2010.

[17] M. Lin and S. Gottschalk, "Collision detection between geometric models: A survey," in *Proc. IMA Conf. Math. Surfaces*, 1998, pp. 602–608.

[18] J. Burgner, P. J. Swaney, R. A. Lathrop, K. D. Weaver, and R. J. Webster, "Debulking from within: A robotic steerable cannula for intracerebral hemorrhage evacuation," *IEEE Trans. Biomed. Eng.*, vol. 60, no. 9, pp. 2567–2575, Sep. 2013.

[19] Y. Guo, J. Granna, K. D. Weaver, R. J. Webster, III, and J. Burgner-Kahrs, "Comparison of optimization algorithms for a tubular aspiration robot for maximum coverage in intracerebral hemorrhage evacuation," in *Proc. Hamlyn Symp. Med. Robot.*, 2015, pp. 11–12.

[20] C. Fellmann and J. Burgner-Kahrs, "Implications of trajectory generation strategies for tubular continuum robots," in *Proc. IEEE/RSJ Int. Conf. Intell. Robots Syst.*, 2015, pp. 202–208.